AN INVESTIGATION ON TEXTURE PROPERTY CORRELATION IN ANNEALED CP-TITANIUM

A Thesis Submitted in Partial Fulfilment of the Requirements for the Degree of

Bachelor of Technology

IN

METALLURGICAL AND MATERIALS ENGINEERING

BY

ROHIT MISHRA (110MM0364)

ABHIJEET DASH (110MM0612)

DEPARTMENT OF METALLURGICAL AND MATERIALS ENGINEERING
NATIONAL INSTITUTE OF TECHNOLOGY
ROURKELA
May, 2014

AN INVESTIGATION ON TEXTURE PROPERTY CORRELATION IN ANNEALED CP-TITANIUM

A Thesis Submitted in Partial Fulfilment of the Requirements for the Degree of

Bachelor of Technology

IN

METALLURGICAL AND MATERIALS ENGINEERING

BY

ROHIT MISHRA (110MM0364)

ABHIJEET DASH (110MM0612)

Under the Guidance of

PROF.SANTOSH KUMAR SAHOO

DEPARTMENT OF METALLURGICAL AND MATERIALS ENGINEERING
NATIONAL INSTITUTE OF TECHNOLOGY
ROURKELA
May, 2014

National Institute of Technology
Rourkela

CERTIFICATE

This is to certify that the thesis entitled, " **An Investigation on Texture-Property Correlation in Annealed CP Titanium"** submitted by **ROHIT MISHRA(110MM0364)**, **ABHIJEET DASH** (**110MM0612**) in partial fulfilment of the requirements for the award of **Bachelor of Technology Degree** in **Metallurgical and Materials Engineering** at National Institute of Technology, Rourkela is an authentic work carried out by them under my supervision and guidance.

To the best of my knowledge, the matter embodied in the thesis has not been submitted to any other University/Institute for the award of any Degree or Diploma.

Date:8/4/14

Prof Santosh Kumar Sahoo

Dept.of Metallurgical and Materials Engineering
National Institute of Technology
Rourkela-769008

ACKNOWLEDGEMENT

We take this opportunity to express our deep regards and sincere gratitude to our guide **Prof. Santosh Kumar Sahoo** for his constant guidance and concern throughout the project. He will always remain be a constant source of inspiration for us. We also express our sincere gratitude to, **Dr. B.C.Ray**, HOD, Metallurgical and Materials Engineering for providing valuable departmental facilities. We are very thankful to **Prof. Indradev Samajdar** of IIT Bombay for his benevolent permission for using the texture facilities at IIT Bombay for conducting experiments. We like to thank **Suryakant Panda** for his help at various stages of the project. We extend our thanks to all the professors who have guided, suggested and helped us during the project. We are also thankful to technical assistants of Department of Metallurgical and Materials Engineering, NIT Rourkela, for their constant practical assistance and help whenever required. We would also like to thank all the staff members of **Metallurgical and Materials Engineering department** and everyone who in some way or the other has provided us valuable guidance, suggestion and help for this project.

ABSTRACT

Rapid industrial development and advances in the fields of engineering and related technologies during the last five decades have led to the extensive use of traditional metals and their alloy counterparts. Ti is one such metal which has gained popularity in the aerospace and defence related applications due to its wide range of mechanical properties like excellent specific strength , stiffness, corrosion and erosion resistance, fracture toughness and capability to withstand significant temperature variations.

The present investigation is a step at correlating the crystallographic orientation and mechanical properties of commercially pure Ti (CP-Ti). Annealed CP-Ti specimens were prepared along the rolling direction, perpendicular to the rolling direction and 45^{o} to the rolling direction. The specimens were then deformed to failure under uniaxial tension test in tensile test. Crystallographic textures of the specimens were measured before and after tensile deformation. Correlation of texture and mechanical properties was investigated. Subsequently, hardness of different grains/orientations of CP-Ti was measured through nano-indentation, grain average misorientation, elastic stiffness and Taylor factor measurements.

KEYWORDS: CP-Ti, Orientation, Texture, Nano-indentation, elastic stiffness, taylor factor

CONTENT

List of Tables

List of Figures

CHAPTER I

1.0 INTRODUCTION

Over the past few decades, Ti and its alloys have come up as a preferred choice of use, because of their superb mechanical properties like, high strength per unit weight, stiffness, commendable erosion and corrosion resistance, fracture toughness and the ability to sustain huge temperature variations [1,2]. Continuous research in the field of material sciences have established Ti as a preferred choice for use in many performance-critical industries like aerospace and defence-related applications [3-4].

Pure Ti melts at 1675^{o}C and weighs atomistically 47.9 amu [5]. The density of pure Ti is 4.5g/cm^{3}, approximately sixty-percent of steel[2, 5]. Furthermore, pure Ti and its alloys have good heat transfer capabilities and non magnetic. The good strength per unit weight of pure Ti at both high temperature (exceeding 590^{o}C) and low temperature (below -253^{o}C) enables it to be the preferred metal that is often chosen and used as an ultrahigh speed metal in aerospace applications like space shuttles ,etc. [3, 5]. The high melting point of Ti metal enables it to be preferred choice for use in turbine engines [6].

Since the Ti metal has excellent superplastic properties, it can be easily deformed to the extent of two-thousand percent without experiencing appreciable necking or cracking when heated to a temperature of 925^{o}C during the super-plastic forming process [6]. Also, Ti and its alloy counterparts are nonmagnetic and have a lower linear coefficient of expansion and lower thermal conductivity than the widely used family of steel and the alloys of aluminium [7]. In more recent years, the automotive industry has increased its use of the Ti metal because of its performance at elevated temperatures coupled with good formability. Noticeably, the metal has minimal degradation and high oxidation resistance during long term service or extended service at elevated temperatures [3, 4].

Essentially, the high cost of producing the Ti metal limited its selection and use to those applications that either required high performance or where life-cycle cost analysis justified its selection and use [8]. It was the aerospace and defences industries that stimulated the initial development of Ti in both commercially pure (CP) form and as alloys in the early 1950's [9, 10]. From a scientific perspective, Ti is categorized as a polymorphic metal because at room temperature [T = 25^{o}C], it has a hexagonal close-packed (HCP) crystal structure, which is referred to as the alpha phase [11]. However, at temperature above 882°C, an allotropic phase transformation occurs to form the body-centered cubic (bcc) crystal

structure, which is referred to as the beta phase [12-14]. Unalloyed Ti is generally referred to as commercially pure (CP) Ti metal, which has noticeably low strength when compared one-on-one to alloys, but is the most corrosion resistant version of the metal [13, 14], making it a preferred choice for military aircraft stationed on ships. Interstitial elements, such as oxygen and nitrogen, are beneficial since they tend to contribute to strengthening of the commercially pure Ti and its different grades [15]. Since commercially pure Ti has excellent corrosion resistance, it is used on-board kitchens, toilets and de-icing equipment.

Helicopters use Ti alloys in highly stressed components like rotor head and rotormast. In space vehicles, Ti alloys are used for the fuel and satellite tanks due to its light weight, high strength and long term chemical compatibility [1, 4]. The automotive industry was attracted to Ti alloys for its light weight, high specific strength (σ/ρ), high elastic energy absorption capacity and excellent corrosion resistance [4]. It is used in exhaust systems, valves, valve cups, connecting rod, turbochargers, suspension springs, etc [5]. The Marine and energy industries require materials having

(a) High corrosion resistance,

(b) Wide range of strength and performance characteristics under static, cyclic and dynamic loading conditions,

(c) Cold resistance in a temperature range of -50°C,

(d) High erosion resistance and fire resistance, which they found the alloys of Ti to meet all of the requirements [6, 16].

Biomedical applications rely on biocompatibility of Ti alloys. Hip and knee-joint prostheses and other permanent implants like casing for cardiac pacemakers, bond fixtures, orthodontic and dental implants are made from the Ti metal [2, 7, 16].

Though Ti and its alloys are expensive, it cannot be compromised on account of its varied properties, low maintenance and long life usage. Ti is expensive due to its high affinity for oxygen creating problems both during extrusion and downstream processing. This limitation has started a considerable amount of scientific and technological interest in developing potentially viable and economically affordable manufacturing methods that aid in reducing the cost of the product.

1.1 OBJECTIVES

The various objectives which are to be achieved in the projects are:

- Determination of mechanical properties such as tensile strength, yield strength and hardness of all the Ti samples.
- Correlation between texture and mechanical properties of Ti samples.

1.2 FRAMEWORK OF THE THESIS

The thesis is divided into five chapters. Chapter I mainly concerns about the introduction of the project work. Chapter II gives theoretical overview of Ti, methods of representing texture, development of texture in Ti and properties of CP Ti. Chapter III represents the details of Ti and sample preparation followed by characterization techniques used in the present investigation. Chapter IV basically tells the results that are obtained by texture measurements, hardness and tensile test measurements and discussion of the experimental results obtained. Chapter V summarizes the results obtained from the present study and hints the scopes for further works

CHAPTER 2

2.1 CP-TI AND ITS METALLURGY

The physical metallurgy of Ti alloys is portrayed in this segment with the exceptional stretch on the different evaluations of commercially pure Ti (CP-Ti). These kind of alloys are focused around the low temperature, hexagonal allotropic manifestation of it. Substitutional alloying components (Aluminium or Tin) or interstitial components (O, C or N) dissolvable in the hexagnal α- phase are available in it. Further particular alloys have been intended to meet the particular end utilization like enhancing ecological safety or diminishing expense and so forth. This has prompted the expansion of the evaluations prompting 16 identifiable alloys or evaluations.

The phenomenal corrosion safety of CP Ti has made it an appealing material of development for substance and petrochemical handling supplies [18]. It additionally has gotten prevalent for heat exchangers and other channeling provisions in light of its weldability and great general fabricability, both in tubing and the resulting forming of the tubing for particular requisitions [19]. In spite of the fact that CP Ti is highly exorbitant at the beginning than SS, articles a product of it frequently have easier life cycle cost in light of the prevalent solidness of CP Ti in administration [20]. CP-Ti is typically chosen for utilization for different requisitions because of its corrosion safety and fabricability, yet different evaluations of Ti are some of the time chose because of absence of quality in CP-Ti needed for the provision. With the developing number of requisitions where mechanical properties are of prime essentialness it is basic for the configuration architect to settle on a prudent decision when selecting materials, e.g motor impellers

The properties of α phase Ti alloys are dependent on constitution and processing history as these control the grain size and preferred orientation when compared with α+β and β alloys. The elastic modulus and yield strength varies between transverse and longituditnal directions in case of sheet products [21]. It varies because of crystallographic texture available. The elastic constants are higher along the c-axis than perpendicular to it. Elastic modulus increases with increase in Al content but oxygen has no impact on it (Table 1). The basic theories for strengthening α phase alloys are solid solution strengthening, both by interstitials and substitutional elements, grain size strengthening, texture strengthening, and precipitation hardening by α_2 phase formation. The strengthening theories relevant to α Ti alloys are given

in Table 2. These strengthening mechanisms sometimes lead to strain localization restricting the operation of deformation twinning and reducing formability.

Table 1 Properties of CP Ti

Material	E (GPa)	$\sigma_{0.2}$ (MPa)	UTS(MPa)	Elongation%	σ_{10^7}(MPa)	$\sigma_{10^7}/\sigma_{0.2}$
Grade 1	105	170	240	24	-	-
Grade 2	105	275	345	20	-	-
Grade 3	105	380	445	18	280	0.73
Grade 4	105	480	550	15	350	0.73

Table 2 Strengthening mechanisms Ti alloys

Strengthening Mechanism	Dependence	Examples/Limitations
Grain Size	$d^{-1/2}$	Fine grains limit twinning
Interstitial Solid Solution	$c^{1/2}$	Strain localization>2500 ppm O_2
Substitutional Solid Solution	c	Strain Localization>5%Al.eq
Texture	c-axis orientation	Max. Strength when loaded along c-axis
Precipitation	$r^{1/2}$, $f^{1/2}$	Occurs> 5.5 % Al.eq

CP-Ti grades are produced in the form of coil. During coiling, the rolling is single directional and the texture is due to working practice. The typical texture present in CP Ti has the maximum concentration of basal pole lying along the direction that connects the sheet normal and width (transverse direction). The point of maximum basal pole concentration is inclined about 30 degrees away from the sheet normal toward the transverse direction. A typical basal pole figure for CP Ti is shown in Fig.1 [22]. The texture in CP Ti is different from the texture in flat rolled α+β alloys due to the absence of twinnig.

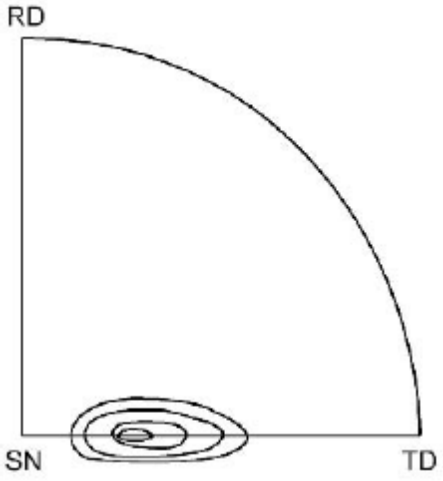

Figure 1 Crystallographic texture CP-Ti sheet[12]

Table 3 Industrial uses for Ti

Industry	Equipment	Environment
Power Generation	Heat-exchangers, Flue Gas Scrubbers, Condensers	Aqueous Solution of various purity,SO_2 containing gases
Water Plants	Desalinization heat-exchangers	Sea water
Petrochemical industry	Heat-exchangers, pipe ,well heads, and down hole hardware	H_2S containing brines
Pulp and paper	Diffusion washers in bleaching section of process	Chlorides containing liquids
Chemical industry	Dimensionally stable electrodes	Cl_2 and Cl_2 compounds
Metal production	Cathodes for electro winning Cu, Au, and Zn	Various aggressive aqueous solutions
Mineral dressing	Pressure vessels at high T and P	Various aggressive aqueous solutions
Biomedical devices	Orthopaedic implants, surgical implants, surgical implements	Human body and autoclave sterilizers
Spacecraft	Cryogenic tanks	N_2O_4, liquid O_2, liquid H_2

2.2 CRYSTAL STRUCTURE

Ti changes by allotropic phase change at 882.5 °c, transforming from a closed packed hexagonal crystal structure (α phase) to body-focused cubic crystal structure (β phase). The definite change temperature is impacted by interstitial and substitutional components. The hcp unit cell of the low temperature α phase is demonstrated in Figure 2a. The ensuing proportion c/a = 1.587 for pure α-Ti is more modest than the perfect degree for a hexagonal closed packed crystal structure with c/a = 1.633. The unit cell of the bcc β phase is demonstrated in Figure 2b. The anisotropic conduct of the α phase has a far reaching impact on the versatile and plastic deformation model of Ti and its alloys. The variety of Young's modulus E of pure α-Ti single crystals at room temperature as a capacity of the angle γ between the c-axis of the unit cell and the stress axis is demonstrated in Figure 3 [23], prompting modulus varieties between 145 Gpa (stress axis ∥c-axis) and 100 Gpa (stress axis ⊥c axis). These sorts of varieties are seen in the worth shear modulus G for shear stresses connected on distinctive planes, despite the fact that such contrasts are less in polycrystalline α-Ti however it can build with profoundly textured material. The flexible moduli have a straight diminishing pattern with expansion in temperature upto conversion temperature. For polycrystalline α-Ti without composition the Young's modulus drops from about 110 Gpa at

RT to something like 58 Gpa simply underneath the transus, while the shear modulus diminishes from something like 42 to 20 Gpa in the same temperature interval[24]. Since the β phase of pure Ti can't be held at RT, Young's modulus qualities are demonstrated here for binary Ti-V strong result alloys in Figure 4. The moduli of β-Ti increment with expanding solute substance and their qualities are much lower as contrasted with those of α- Ti.

2.2.1 DEFORMATION MODES

The observed ductile behaviour of α-Ti, also at low testing temperatures, results from the combined contribution of slip and twinning modes.

Slip system	Burgers vector type	Slip direction	Slip plane	No. of slip systems total	independent
1	$\vec{a}$	$<11\bar{2}0>$	(0002)	3	2
2	$\vec{a}$	$<11\bar{2}0>$	$\{10\bar{1}0\}$	3	2
3	$\vec{a}$	$<11\bar{2}0>$	$\{10\bar{1}1\}$	6	4
4	$\vec{c}+\vec{a}$	$<11\bar{2}3>$	$\{10\bar{1}1\}$	12	5

Table 4 Slip systems in the hcp α phase[15]

2.2.1.1 SLIP MODES

The various slip systems observed in α-Ti are listed in Table 4 and respective slip planes and slip directions in the hcp unit cell are shown in Figure 5. The three slip systems in Table 4, which all have the same type of Burgers vector, together, possess nominally 8 independent slip systems. However, this number reduces to only 4 systems due to the changes of shape that can be produced by the combined slip systems 1+2 are exactly the same as those of the slip system 3. In no case is an extension parallel to the c-axis possible. Therefore, in order to satisfy the von Mises criterion, which requires at least five independent slip systems for a homogeneous plastic deformation of polycrystals, the operation of one of the slip systems $\{10\bar{1}1\}$ with a $\bar{c}+\bar{a}$ Burgers vector needs to be activated, which has been observed in a number of Ti-alloys [14, 15]. The predominant slip mode in α-Ti is $\{10\bar{1}0\}$ $<11\bar{2}0>$, followed by $\{10\bar{1}1\}$ and (0002) both with an $\bar{a}$ type Burgers vector. The highest critical resolved shear stress (CRSS) is required for slip with $\bar{c}+\bar{a}$ Burgers vector. Absolute values of CRSS are strongly dependent on alloy content and on test temperature. An example of CRSS for three different slip systems in solid solution strengthened Ti-Al single crystals as a function of test temperature is shown in Figure 6 [16].

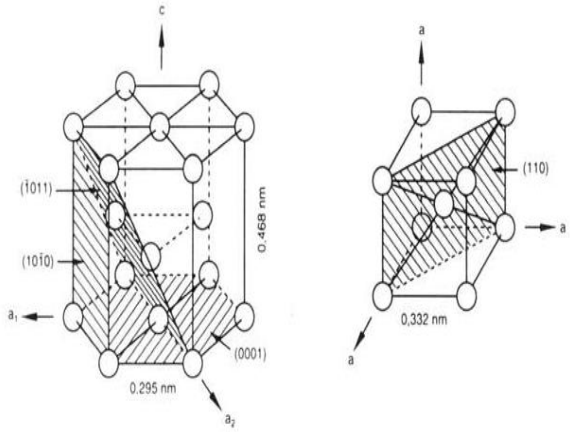

Figure 2 Unit cells of α and β phases

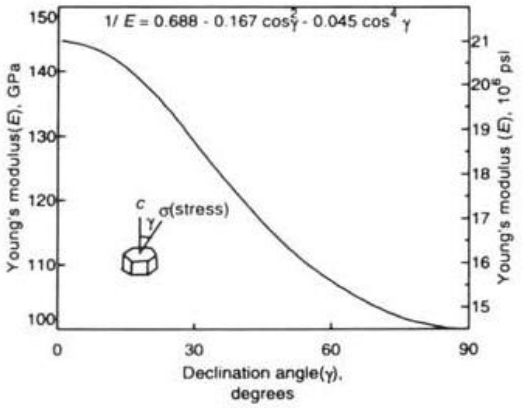

Figure 3 Variation of young's modulus with declination angles

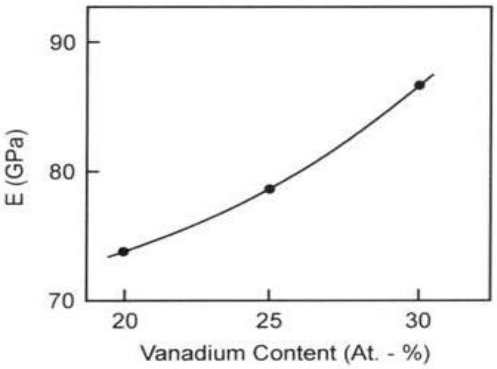

Figure 4 E = f(vanadium content) [15]

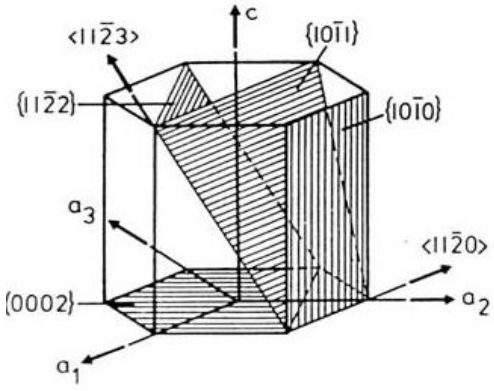

Figure 5 slip directions and slip planes in hcp α phase[15]

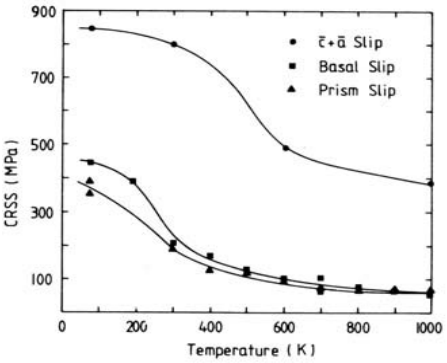

Figure 6 CRSS of slip with burgers vector[15]

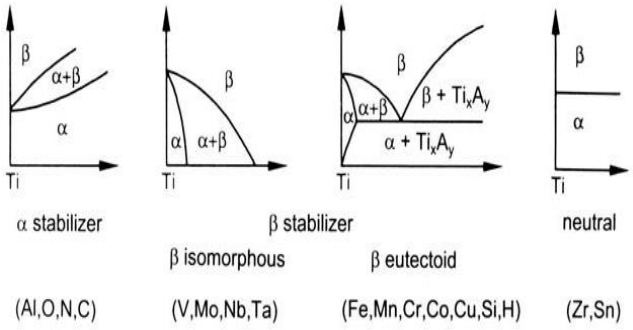

Figure 7 Influence of alloying elements[15]

2.2.1.2 DEFORMATION TWINNIG

There are many twinning modes observed in Ti [12]. The {1121} twins allow an extension along the c-axis, while the {1122} twins permit a reduction[14]. Therefore, twinning is dependent on the sense of the applied stress, in contrast to plastic deformation by dislocations. Increasing contents of solute atoms are suppressing twinning, such as oxygen or aluminum, therefore twinning as a deformation mode to allow a shape change parallel to the c-axis of a-Ti plays only a role in pure or commercial purity Ti with lower oxygen

concentrations [14]. Twinning is also drastically reduced with decreasing grain sizes or phase dimensions [12].

2.2.2 PHASE DIAGRAMS

Alloying components in Ti are considered α or β stabilizers on the premise of their consequences for the α to β conversion temperature or on their contrasting solubilities in the α or β phases. The substitutional component Al and the interstitials O, N and C are solid α stabilizers and expansion the transus temperature with expanding solute content, as indicated in Figure 7. The β-balancing out components bring down the transus temperature. These are recognized into β-isomorphous sorts (e.g. V, Mo, Nb, Ta) and β-eutectoid sorts (e.g. Mn, Fe, Cr, Co, Ni. Cn, Si, H). What's more, there exist different components, for instance Zr and Sn, which carry on pretty much impartial or are marginally diminishing the transus temperature (Figure 7). Actual equilibrium phase diagrams for all of these systems can be found in [18].

2.2.2.1 PHASE TRANSFORMATIONS

The transformation of the bcc β to the hcp α structure by freezing through the transition temperature occurs by a nucleation and shear type process. The crystallographic direction relation between α and β has first been studied for Zr by Burgers [19], and is therefore named Burgers-Relationship:

$$\{110\}_\beta \,//\, (0002)_\alpha$$

$$<111>_\beta \,//\, <11\bar{2}0>_\alpha$$

This relationship was confirmed later also for Ti [20]. According to this relationship a bcc crystal can therefore transform to 12 hexagonal variants, having different orientations with regard to the parent β crystal. This transformation can occur either martensitically or by a nucleation and growth process, depending on alloy composition and cooling rate.

2.2.2.2 ALLOY CLASSIFICATION

Ti alloys are separated customarily into three separate sorts as α, α+β, and β alloys as per their equilibrium constitution, which shifts with the sorts and amassings of alloy components. This is indicated in a schematical pseudobinary β-isomorphous phase graph in Figure 10. Ti having different measures of interstitial oxygen to enlarge the yield stress and alloys with α stabilizers (Al, Sn) having hcp crystal structure at low temperature are considered α alloys. These alloys hold, notwithstanding the α stabilizer Al, additionally β balancing out components, for example, V, Mo, Nb or Cr. These components diminish the α to β change temperature and expansion the width of the α+β phase field with expanding β-solute content. Additionally they bring down the temperature, when the β phase begins to convert by the martensitic methodology. With a further expand in β balancing out components, past that

level which brings down the Ms-temperature to RT, those alloys are then called metastable β alloys. For these alloys the β phase might be held at RT even in extensive segments throughout air cooling. In any case, these metastable β alloys can generally be changed to a α+β mixture by isothermal maturing. At significantly higher β stabilizer substance the alloys are steady β alloys, which can't be changed to a α+β mixture by further heat treatments.

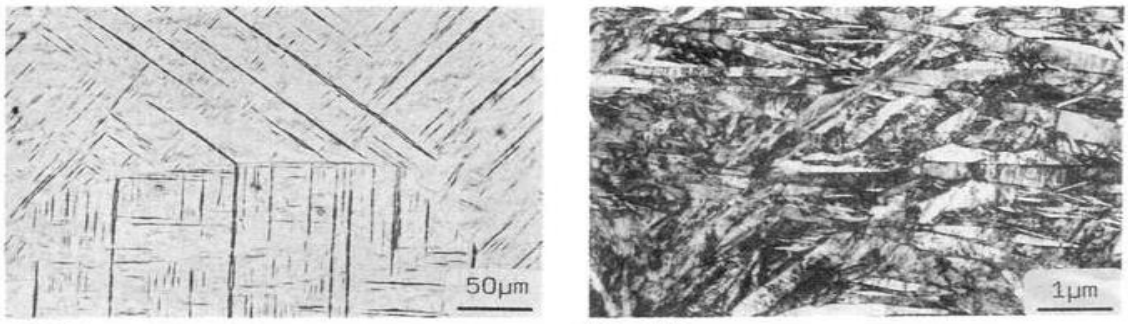

Figure 8 Acicular martensite structure[15]

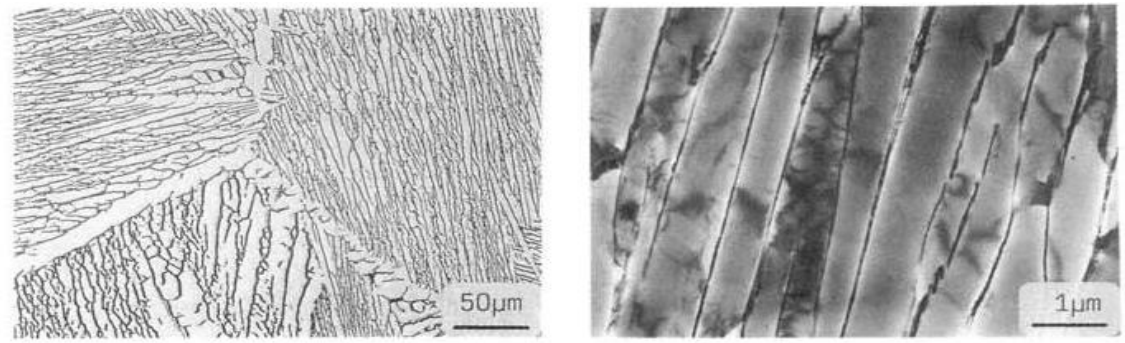

Figure 9 Lamellar α+β microstructure in Ti-6Al-4V slowly cooled from the β phase field[15]

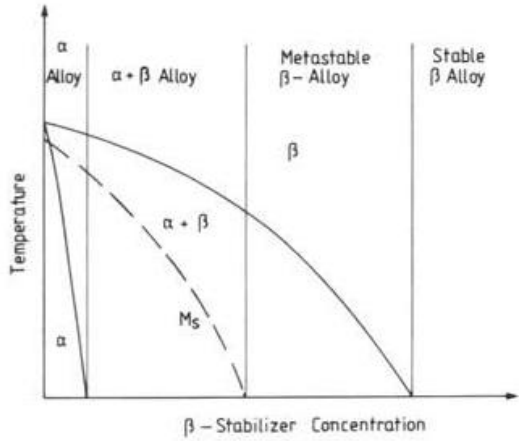

Figure 10 Pseudobinary β isomorphous phase diagram [15]

2.3 TEXTURE

Crystallographic orientation or simply orientation means the relative positioning of atomic plane in a crystal to a fixed reference. Even though grain orientations are highly unlikely to be randomly distributed but crystallization from melt to solid state and thermomechanical processing increase the likely development in certain patterns in orientation. This tendency is known as texture. Texture is very important as it influences the material properties. Indeed, it has been found that the influence of texture on material properties is, in many cases, 20%–50% of the property values [33].

The direction of any 3-D vector in a crystal—a crystallographic direction or the ordinary to a crystal plane—might be depicted as a point on the unit reference circle, that is, a circle with span 1 notionally living around the crystal . As an illustration, Figure 11 shows the (0001) plane in a hexagonal crystal. The purpose of crossing point of the typical to this plane with the reference circle, that is, its post, is a measure for the game plan of this plane in the crystal. Gave that the reference unit circle is appended to an outer edge, the position of the shaft on the circle additionally gives data on the crystallographic introduction of the crystal concerning this casing, in spite of the fact that the crystal has still one level of flexibility by turning around this specific pivot. In crystallography and metallurgy, most generally the stereographic projection is utilized, the guideline of which is indicated in Figure 12 has a tendency to be more famous

2.3.1 THE POLE FIGURE

The projection of poles onto a pole figure from a reference figure is appeared. The position of the obliged pole on the circle is resolved as far as two angles (Hansen et al., 1978): The angle α is the azimuth of the pole, where north pole is given by α = 0° and the angle β describes the rotation of the pole around the polar pivot, beginning from a specified reference bearing (Fig 11). For the characterisation of the crystallographic orientation the exceptional game plan is dead set as far as the angles α and β concerning an outside reference frame, that is, the example or specimen coordinate framework S. For instance while rolling the sheet normal course ND is ordinarily decided to be in the north pole of the circle, with α = 0° for ND, and the rotation angle β is 0° for the rolling heading RD or, less every now and again, the transverse bearing TD. For other deformation modes or example geometries a fitting 3-D, ideally right-handed, coordinate framework must be determined.

.

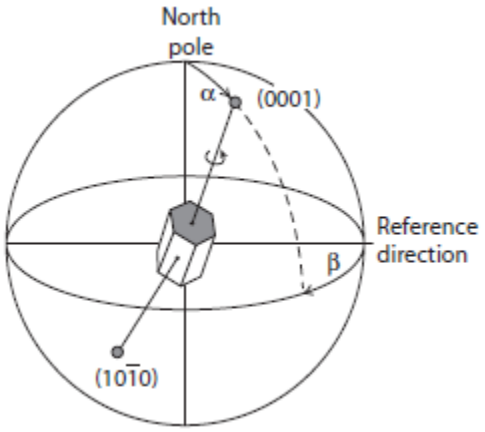

Figure 11 Orientation in hexagonal crystal (basal plane)[29]

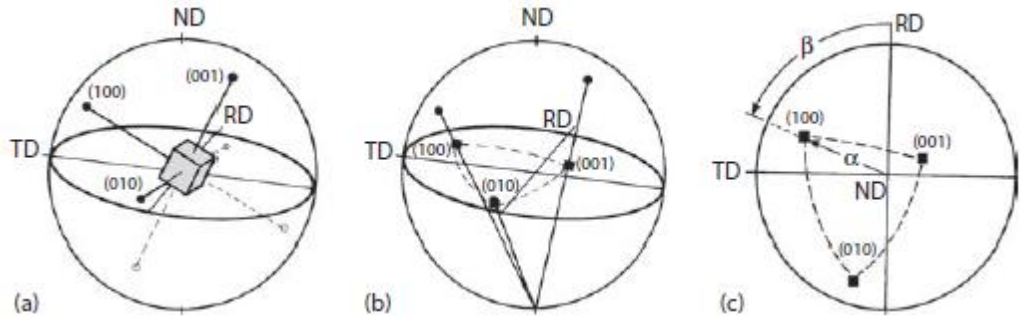

Figure 12 Illustration of the {100} poles [29]

The reference system of the pole figure is the specimen coordinate system S which is determined by the specimen axes $\{s_1s_2s_3\}$, and the crystal orientation given by the axes of the crystal coordinate system C = $\{c_1c_2c_3\}$ is projected into this frame. If R is a vector parallel to the pole of interest (XYZ), then it can be expressed in the two frames S and C according to

$$R = s_1 \sin\alpha\cos\beta + s_2 \sin\alpha\sin\beta + s_3 \cos\alpha$$

and

$$R = \frac{1}{N}(c_1X + c_2Y + c_3Z)$$

(*XYZ*) are the coordinates of the pole in the crystal frame, for example, (111), and *N* is a constant with $N = \sqrt{X^2 + Y^2 + Z^2}$ to normalize *R* to unity. Scalar multiplication of above equations in succession by the three vectors s_1 under consideration of the definition of an orientation finally yields

$$\begin{matrix} sin\alpha cos\beta \\ sin\alpha sin\beta \\ cos\alpha \end{matrix} = \frac{1}{N}\begin{pmatrix} g_{11} & g_{21} & g_{31} \\ g_{12} & g_{22} & g_{32} \\ g_{13} & g_{23} & g_{33} \end{pmatrix}\begin{pmatrix} X \\ Y \\ Z \end{pmatrix}$$

(note that $g^t = g^{-1}$ shows up here). Above mathematical statement yields nine equal statements to determine the pole figure angles α and β for a given pole (XYZ) from the orientation lattice g (Hansen et al., 1978). Just distinctive poles were recognized. Nonetheless, as officially said, one pole does not yield the whole orientation data, since the crystal can at present turn about this specific pole (Fig 13). Consequently, the dissemination of the c axes in a hexagonal material, that is, its (0001) pole figure, does not give an unambiguous representation of the surface of the example; different poles must be acknowledged to speak to unambiguously an orientation. In this illustration, the extra data about the position of, say, the (1010) pole might focus the orientation in an unequivocal way (Fig 13). In spite of the fact that in this illustration the orientation is completely described by two poles, all in all—contingent upon the symmetry of the crystal or the poles—three poles are important to determine totally the orientation grid g. Normally, the extra data is given by different poles of the same group of planes, that is, diverse poles (hkl) of the family {hkl}. For example, the hexagonal crystal has three equal {1120} planes, (1120), (1210), and (2110), so that every orientation in the comparing {1120} pole figure is precisely portrayed by the relating three poles. In pole figures like {1121} and {1101}, any orientation is characterized by six comparable poles. In cubic crystals, a given orientation is depicted by (not numbering the same poles with negative signs) three {100}, four {111}, six {110}, twelve {012}, {112}, {113}, and so on., and—in the most general case— twenty-four {hkl} poles, which implies that all pole figures of cubic crystals include enough poles to depict unambiguously an direction

2.3.2 THE INVERSE-POLE FIGURE(IPF)

Instead of depicting the orientation of the crystal-coordinate system in the specimen-coordinate system, that is, in a pole figure, vice versa the orientation of the specimen-coordinate system can be projected into the crystal-coordinate system. This representation is called the inverse pole figure. Thus, the reference system of the inverse pole figure is the crystal coordinate system C, and the "orientation" is defined by the axes of the specimen coordinate system S, for example, RD, TD, and ND. In an analogy to previous Equation
where the pole figure angles α and β of a unit vector parallel to the crystallographic axis (XYZ) have been considered in the frame S, now the angles γ and δ of a vector parallel to a specimen axis s_i in the coordinate system C must be introduced:

$$s_i = c_1 \sin\gamma_i \cos\delta_i + c2 \sin\gamma_i \sin\delta_i + c3\cos\delta_i$$

Scalar multiplication now leads to

$$\begin{matrix} sin\gamma cos\delta \\ sin\gamma sin\delta \\ cos\delta \end{matrix} = \begin{pmatrix} g_{11} & g_{21} & g_{31} \\ g_{12} & g_{22} & g_{32} \\ g_{13} & g_{23} & g_{33} \end{pmatrix} \begin{pmatrix} X_s \\ Y_s \\ Z_s \end{pmatrix}$$

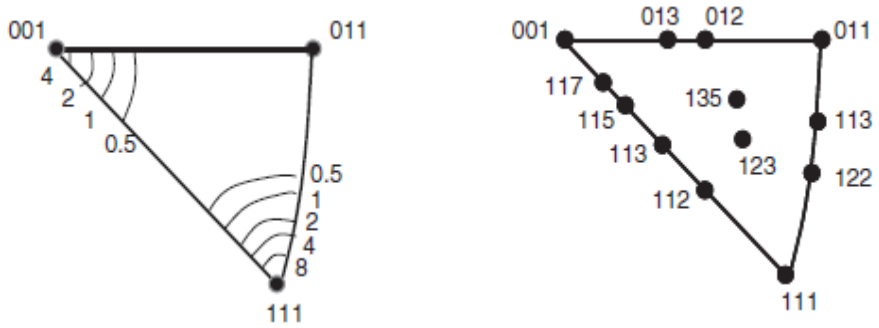

Figure 13 The [001][011][111] unit triangle; and inverse pole figure using the unit triangle to indicate with the help of contour plots how intense a particular crystallographic direction is oriented parallel with an external reference direction[29]

These statements depict the components of the orientation grid g as far as the position of the example axes. IPF are regularly utilized for axial symmetric examples, where one and only of the axes is endorsed. Case in point, for tensile or compression or examples the orientation progressions of the compression or tensile pivot are plotted in the crystal direction framework. As indicated by the crystal symmetry it is not important to show the whole pole figure, however a single unit triangle will be enough.

2.3.3 THE EULER ANGLE AND EULER SPACE.

Generally, the three rotations are expressed as

$$g_{\omega 1} = \begin{pmatrix} cos\varphi_1 & sin\varphi_1 & 0 \\ -sin\varphi_1 & cos\varphi_1 & 0 \\ 0 & 0 & 1 \end{pmatrix}$$

$$g_{\Phi=} \begin{pmatrix} 1 & 0 & 0 \\ 0 & cos\Phi & sin\Phi \\ 0 & -sin\Phi & cos\Phi \end{pmatrix}$$

$$g_{\omega 2} = \begin{pmatrix} cos\varphi_2 & sin\varphi_2 & 0 \\ -sin\varphi_2 & cos\varphi_2 & 0 \\ 0 & 0 & 1 \end{pmatrix}$$

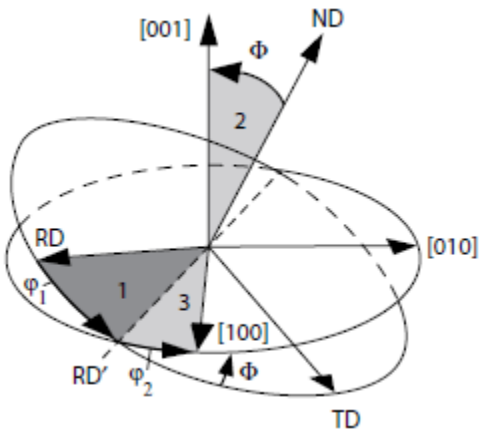

Figure 14 Rotation between specimen and axes described by Euler Angles[29]

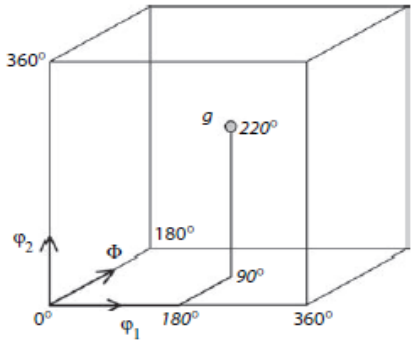

Figure 15 Representation of the necessary orientations defined by Euler angles (Bunge Convention)[29]

				Sample Symmetry		
		Crystal Symmetry		Orthonormal	Monoclinic	None (Triclinic)
Crystal System	Laue Class	Φ	φ_2	φ_1	φ_1	φ_1
Triclinic	$\bar{1}$	180°	360°			
Monoclinic	2/m	180°	180°			
Orthorhombic	mmm	90°	180°			
Trigonal	$\bar{3}$	180°	120°			
	$\bar{3}$m	90°	120°	90°	180°	360°
Tetragonal	4/m	180°	90°			
	4/mmm	90°	90°			
Hexagonal	6/m	180°	60°			
	6/mmm	90°	60°			
Cubic	m$\bar{3}$	90°[a]	180°			
	m$\bar{3}$m	90°[a]	90°			

Table 5 Size of the Euler Space Necessary to Represent Unequivocally Orientations[29]

2.4 X RAY DIFFRACTION

The crystallographic orientation of a crystalline sample can be determined by X-Ray diffraction. Earlier the orientations were determined by studying the inhomogeneous peak distribution along Debye Scherrer rings. Present day X-Ray diffraction use texture goniometer and Geiger counters. This method can be employed for all kinds of materials except for materials with multiphase systems and materials with low crystalline symmetry.

Generally a X-Ray system has the a a X-ray tube,X-ray generator,goniometer with a sample stage and a detection system. The following is of a texture goniometer.

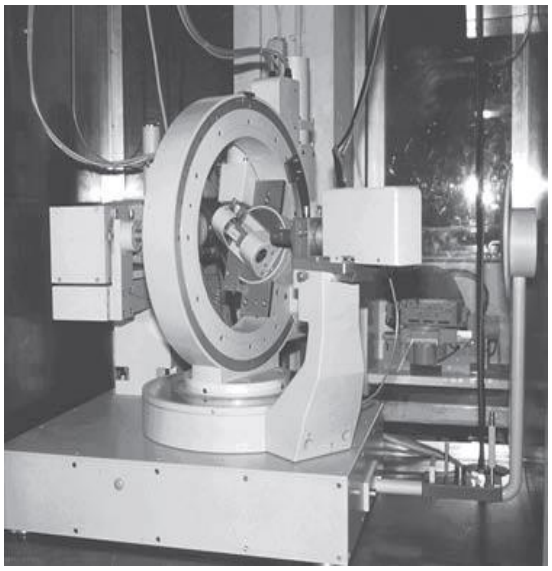

.

2.4.1 POLE FIGURE DIFFRACTOMETRY

A pole-figure goniometer contains a four-axis single crystal diffractometer. The detector is placed at the required Bragg angle with respect to incident x ray beam. The sample is placed relative to 3 $\perp$ axes ω φ and χ; the ω axis coincides with θ as shown in the figure. The diffractometry can be done in 2 modes

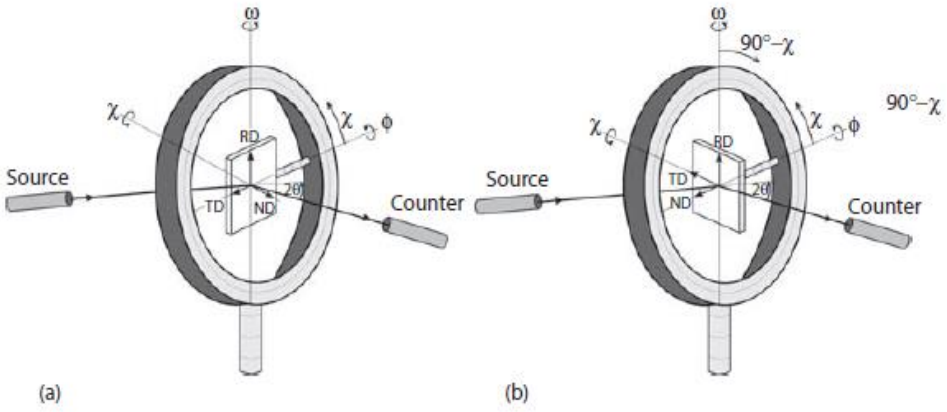

Figure 16 Different Modes of Pole figure diffractometry

2.4.2 POLE FIGURE SCANNING

The goniometers that are regulated by a single motor, the pole figures are examined by changing both α & β at the same time. An electrical counter measures the reflected intensity for each point (α,β). There are two different methods of pole figure scanning.

1. Step scanning mode- Here the intensities are measured after rotating the samples by a particular angle on a spiral or continuous axis. The values are taken after the specific interval of angles.
2. Continuous scanning mode-Here the values are measured continuously over the given range and integrated . The scanning grid has to be continuous in this case.

.2.5 ELECTRON BACKSCATTER DIFFRACTION(EBSD)

Electron backscatter diffraction (EBSD) or backscatter Kikuchi diffraction (BKD) is a microstructural crystallographic procedure. It is utilized to focus the crystallographic introduction of numerous materials, which might be utilized to depict surface or favored introduction of any crystalline or polycrystalline material. EBSD can list and distinguish all the seven crystal frameworks. Thus it is connected to crystal introduction mapping, stage recognizable proof, deformity studies, grain limit and grain morphology studies, local heterogeneity examinations, material separation, mapping micro strain, and utilizing reciprocal techniques,and physicochemical ID. Traditionally these sorts of studies have been done utilizing X-beam diffraction (XRD), neutron diffraction and/or electron diffraction in a TEM.

Electron Backscattered diffraction is carried out utilizing a Scanning Electron Microscope (SEM) outfitted with an EBSD indicator which is associated with a phosphor screen, minimal lens and low light CCD Polaroid chip. Economically accessible EBSD frameworks ordinarily accompany one or two distinctive CCD Polaroids: The CCD chip with a local determination of 640×480 pixels is utilized for quick estimations while for slower, and more delicate estimations, the CCD chip determination can go up to 1600×1200 pixels. Nonetheless, with higher resolutions the readouts are more lengthy. The greatest focal point of the high-determination identifiers is their higher affectability. For composition and introduction estimations, the pictures are binned so as to diminish their size and lessen computational times. Accordingly, the exchange and elucidation of up to just about 1000 pictures/s is conceivable if the diffraction sign is sufficient.

For an EBSD estimation a level/cleaned crystalline example is put in the SEM chamber at an exceedingly tilted point (~70° from flat) towards the diffraction Polaroid, to build the differentiation in the resultant electron backscatter diffraction design. The phosphor screen is spotted inside the example assembly of the SEM at an edge off more or less 90° to the shaft piece and is coupled to a smaller lens which centers the picture from the phosphor screen onto the CCD Polaroid. In such a design a percentage of the electrons entering the example backscatter may escape. As these electrons leave the example, they may retreat at the Bragg condition identified with the dispersing of the occasional nuclear cross section planes of the crystalline structure and diffract. These diffracted electrons can get away from the material and some will impact and energize the phosphor making it fluoresce.

An electron backscatter diffraction design (EBSP) is framed when numerous distinctive planes diffract diverse electrons to structure Kikuchi groups which relate to each of the grid diffracting planes. On the off chance that the framework geometry is generally depicted, it is conceivable to relate the groups introduce in the EBSP to the underlying crystal stage and introduction of the material inside the electron connection volume. Each one band could be recorded independently by the Miller records of the diffracting plane which shaped it. In most materials, just three groups/planes which block are obliged to depict an extraordinary answer for the crystal introduction (based upon their interplanar points) and most business frameworks use find tables with global crystal information bases to perform indexing.

While this "geometric" depiction identified with the kinematic result (utilizing the Bragg condition) is influential and helpful for introduction and composition investigation, it just

depicts the geometry of the crystalline cross section and disregards numerous physical methodologies included inside the diffracting material. To sufficiently portray better characteristics inside the EBSP, one must utilize a numerous pillar dynamical model (e.g. the variety in band intensities in an exploratory example does not fit the kinematic result identified with the structure variations.

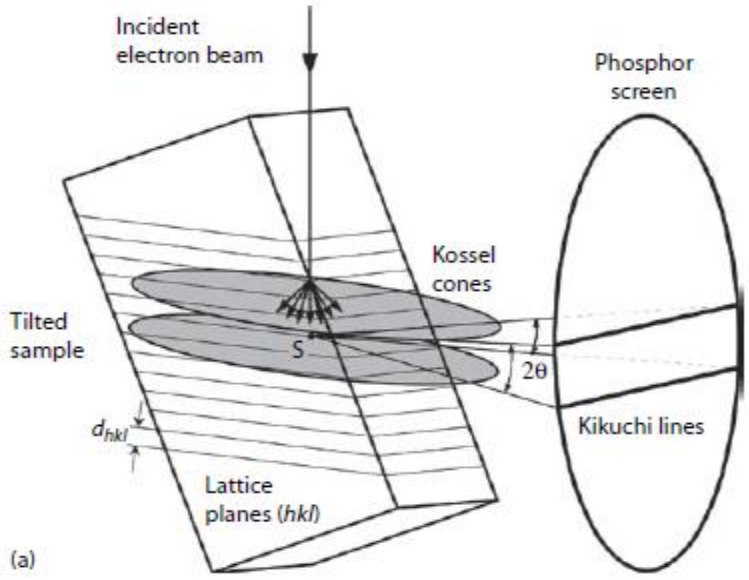

Figure 17 Origin of Kikuchi lines from the EBSD (i.e., tilted specimen) perspective.[29]

2.6 NANO-INDENTATION

The objective of nano-indentation tests is to find out elastic modulus and hardness of the material from load-displacement estimations. Conventional indentation hardness tests include the approximation of the measure of a leftover plastic impression as a capacity of the indenter load. This gives a area of the region of contact for a given indenter load. In a nano-indentation test, the extent of the leftover impression is just a few microns and this makes it largely troublesome to get a exact measure utilizing optical procedures. In nano-indentation testing, the depth of infiltration underneath the example surface is measured as the load is connected to the indenter. The indenter's geometry permits the measure of the range of contact to be resolved.

2.6.2 LOAD-DISPLACEMENT CURVES

The main goal of nano-indentation testing calculates hardness & elastic modulus of the specimen material from experimental readings of indenter load and depth of penetration. In a typical test, force and depth of penetration are recordes as load is applied from zero to some maximum and vice versa. On the off chance that plastic disfigurement happens, then there is a leftover impression left on the surface of the example. Not at all like customary space

hardness tests, the size (and consequently the anticipated contact region) of the remaining impression for nano-space testing is so little it would be impossible measure correctly with optical methods. The profundity of infiltration together with the known geometry of the indenter gives a backhanded measure of the zone of contact at full load, from which the mean contact weight, and in this manner hardness, may be assessed. At the point when burden is evacuated from the indenter, the material endeavors to recover its unique shape, yet it kept from doing so as a result of plastic twisting. Be that as it may, there is some level of recuperation because of the unwinding of versatile strains inside the material. An investigation of the introductory segment of this versatile emptying reaction gives an evaluation of the flexible modulus of the indented material. The type of the consistence bends for the most widely recognized sorts of indenter are very much alike and is demonstrated in figure.

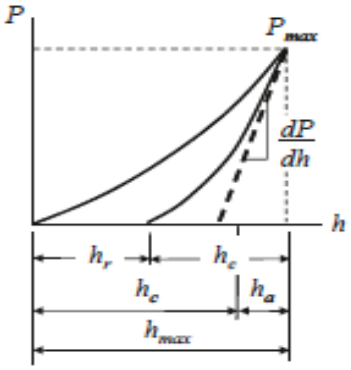

Figure 18 Loading and Deloading (Compliance Diagrams)[30]

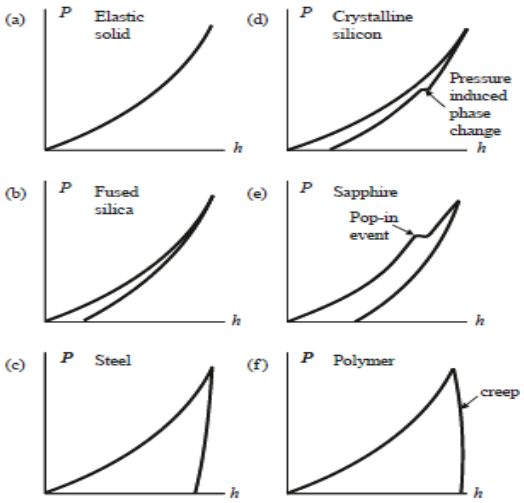

Figure 19 Load displacement diagrams for different materials[30]

CHAPTER III

3.0 MATERIALS AND EXPERIMENTAL PROCEDURE

3.1 MATERIALS

Materials studied (Cp-Ti)in this study were obtained from plates of 0.5mm thickness. Chemical composition (in wt.%) of the plates is given in table 6. The 0.5 mm thickness plates were obtained from 5 mm thick plates after these plates were subjected to cold rolling leading to 90% reduction in thickness in a laboratory rolling mill. The cold rolled sheets were then annealed at 600^{o}C for 1hr in a batch furnace. Tensile specimens of dimension shown in figure, were prepared from the annealed sheets by laser cutting so as to not to introduce any residual stresses. Tensile specimens were prepared with respect to different sample orientations – along rolling direction, along 45^{o} to the rolling direction and along 90^{o} to the rolling direction as shown in figure 21.

Table 6 Chemical composition (in wt.%) of cp-Ti used in the present study

Fe	C	N	H	O	Ti
0.034	0.004	0.004	0.0004	0.134	Balance

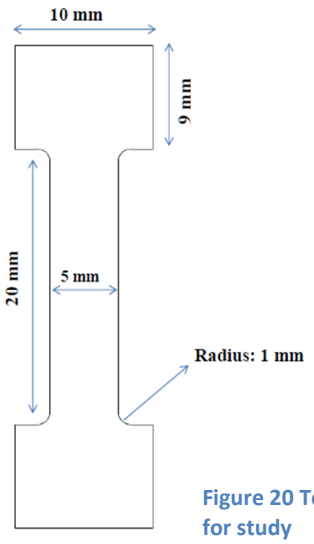

Figure 20 Tensile specimen used for study

3.2 TENSILE TEST

All the samples were subjected to tensile deformation beyond yield point, till ultimate tensile strength and till fracture respectively. Tensile testing was carried out in an Instron 1195. The specimens were metallographic polished before tensile testing and after tensile testing.

3.3 TEXTURE CHARACTERISATION

The specimens were metallographic and electro-polished for XRD (X-ray diffraction), EBSD (Electron backscattered diffraction) and nano-indentation analysis. Standard procedure was followed for metallographic polishing, whereas electro-polishing was carried out in a Struers polisher, LectroPol-5, at 25V for 20sec and the electrolyte used was methanol and perchloric acid (80:20) at a temperature of -20°C.

3.2.1 BULK/MACRO TEXTURE

A Panalytical MRD X-ray diffraction system is used for bulk texture characterization. This is available at IIT Bombay and is used for the present study. Four different pole figures, $(01\bar{1}1)$, $(01\bar{1}2)$, $(01\bar{1}3)$ and $(11\bar{2}4)$ were measured. Subsequently the ODF was estimated using an academic software Labotex.

3.2.2 MICRO TEXTURE

A Fei-quanta SEM (scanning electron microscope) attached with TSL-OIM was used for microtexture characterization. The system is known as electron backscattered diffraction (EBSD) system. This is also available at IIT Bombay and is used for the present study. EBSD was carried out for grain size and grain average misorientation determination. Grain average misorientation (GAM) is the average misorientation between each point in a grain. An approximate area of 1 mm x 1 mm was scanned by the EBSD in each sample. Orientation estimated elastic stiffness of different grains was estimated and also the Taylor Factor was estimated.

3.4 NANO INDENTATION TEST

Nano-indentation was carried out using a nano-mechanical testing instrument, Hysitron Triboindenter (TI 900). A Berkovich diamond indenter was used for indentation. Hardness of more than 300 grains was measured using a load of 9000μN. The load was decided based on the indentation depth.

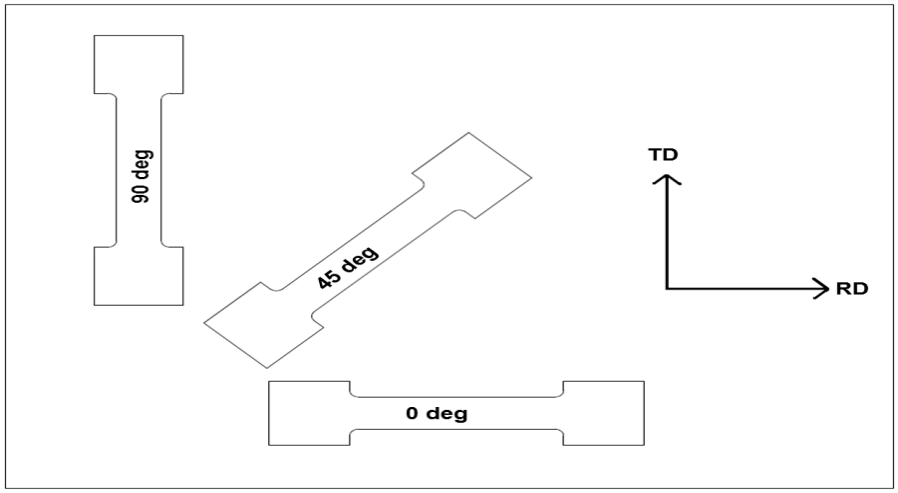

Figure 21 Different oriented specimens used in the study

CHAPTER IV

RESULTS AND DISCUSSION

Mechanical properties of cp-Ti with respect to its orientation (i.e. along rolling direction, 45^{o} to the rolling direction and 90^{o} to the rolling direction) are shown in table 7. The sample has high strength in the rolling and 90^{o} to the rolling direction while the ductility is more in the direction 45^{o} to the rolling direction.

Table 7 Mechanical properties of Ti alloy

SAMPLE	YIELD STRENGTH(MPa)	TENSILE STRENGTH(MPa)	YOUNG'S MODULUS(MPa)	ELONGATION(%)
0 DEG	253	419.72	23733.73	31.56
45 DEG	235	359.102	26050	33.26
90 DEG	328	392.359	33684.77	26.57

Nano-indentation of the cp-Ti sample is shown in figure 22. Initially nano-indentation was performed on different grains according to the points numbered on the sample of an annealed cp-Ti sample. Then the orientation of the same grains where nano-indentation was performed was estimated by the EBSD measurements. The hardness values corresponding to the colour code is shown in table 8. The figure shows that the basal orientations had higher hardness compared to non-basal orientations. The hardness of grains gradually decreased as we moved from the centre of stereographic triangle to the outer sides of it.

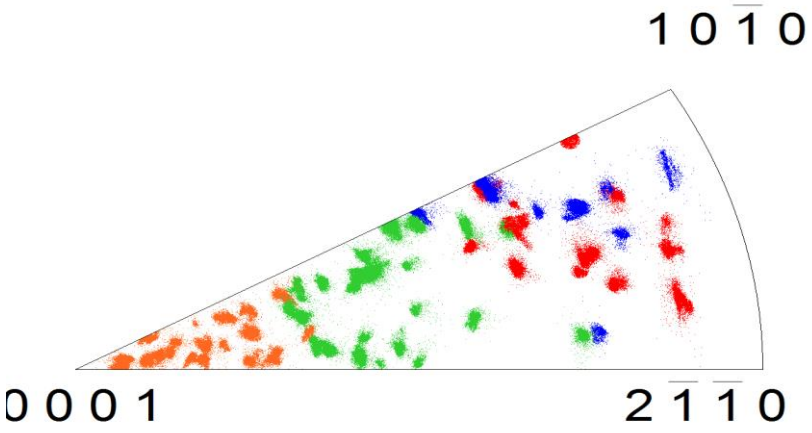

Figure 22 Inverse pole figure showing nano indentation points

Table 8 Nano indentation hardness table

.

Colour code	Hardness value (GPa)	Colour code	Hardness value (GPa)	Colour code	Hardness value (GPa)
1	3.10	1	2.50	1	2.00
2	2.99	2	2.48	2	1.99
3	2.97	3	2.42	3	1.97
4	2.96	4	2.41	4	1.96
5	2.95	5	2.39	5	1.94
6	2.82	6	2.35	6	1.93
7	2.81	7	2.33	7	1.92
8	2.75	8	2.32	8	1.83
9	2.74	9	2.31	1	1.78
10	2.72	10	2.30	2	1.77
11	2.69	11	2.29	3	1.765
12	2.69	12	2.27	4	1.762
13	2.67	13	2.23	5	1.76
14	2.65	14	2.22	6	1.729
15	2.61	15	2.19	7	1.724
16	2.59	16	2.17	8	1.70
17	2.59	17	2.15	9	1.69
18	2.58	18	2.07	10	1.68
19	2.58	19	2.04	11	1.675
20	2.57	20	2.03	12	1.673
21	2.57	21	2.01	13	1.66
22	2.55			14	1.64
23	2.53				
24	2.52				

To quantify the extent of deformation the grain average misorientation, grain oriented elastic stiffness and Taylor factor was calculated for 0 deg sample for 3 different conditions (i) deformed till yield point, (ii) deformed till ultimate tensile strength and (iii) deformed till fracture. In all the three cases the values were shown to increase with the deformation. In all the cases except Taylor factor the average values are seen to be increasing as we move from the stereographic centre towards the outer region of the triangle. The average values are presented in colour coded table.

GRAIN AVERAGE MISORIENTATION

(i) Deformed till yield point

COLOUR CODE	AVERAGE GAM
	0.71
	0.87
	1.34

(ii) Deformed till ultimate tensile strength

COLOUR CODE	AVERAGE GAM
	0.92
	1.34
	1.48

(iii) Deformed till fracture

COLOUR CODE	AVERAGE GAM
	1.04
	1.37
	1.58

ELASTIC STIFFNESS

COLOUR CODE	AVERAGE
	82.19
	142.76
	103.19

TAYLOR FACTOR

COLOUR CODE	AVERAGE
	3.06
	2.76
	1.46

Bulk texture developments in cp-Ti w.r.to its orientation (i.e. along rolling direction, 45^{o} to the rolling direction and 90^{o} to the rolling direction) is shown in figure 23, 24 & 25. This

shows a significant near basal texture in all the samples. The volume fraction of basl texture is maximum in 0 deg sample followed by 90 deg and then 45 deg.

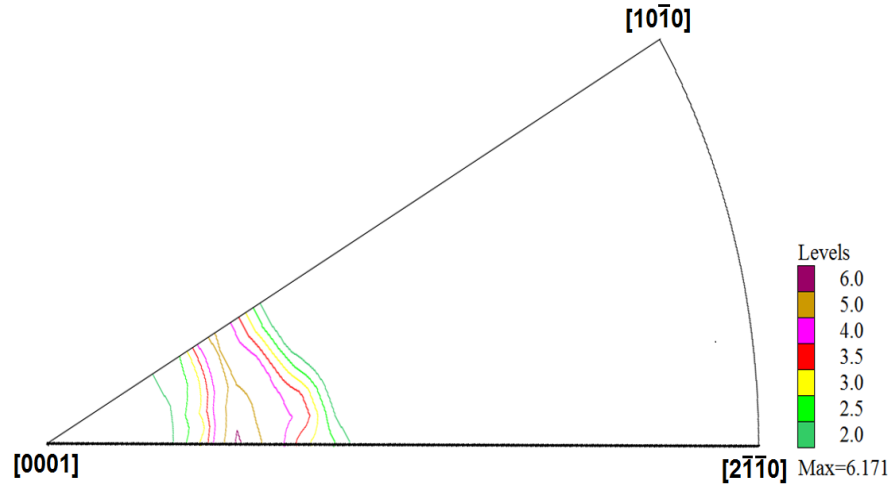

Figure 23 Inverse pole figure showing bulk texture of sample oriented towards the rolling direction

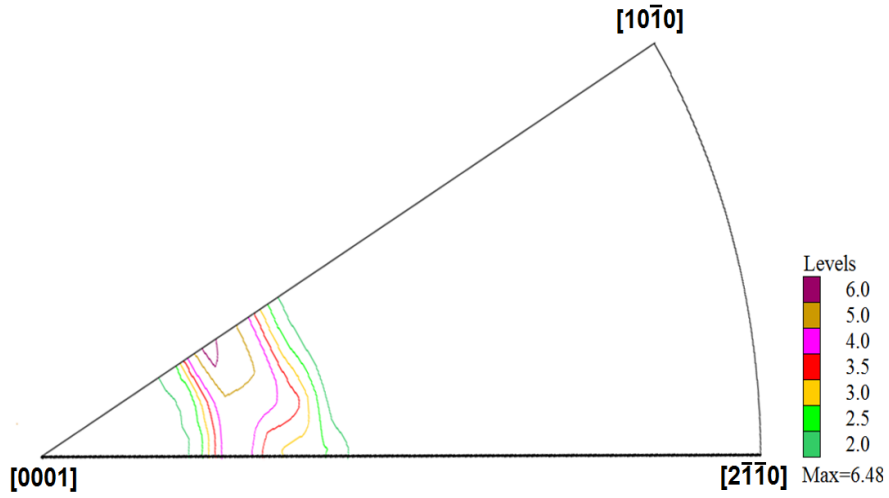

Figure 24 Inverse pole figure showing bulk texture of sample oriented 45 deg to the rolling direction

Figure 25 Inverse pole figure showing bulk texture of sample oriented 90 deg to the rolling direction

CHAPTER V

The Hardness and Mechanical properties of Cp-Ti sheets in rolling direction, 45^{o} to rolling direction and 90^{o} rolling direction is checked and the following conclusions are drawn

- The basal/near basal orientations are the hardest orientations in annealed cp-Ti.
- The GAM (a measure of misorientation in a grain) development was lower in basal/near-basal grains during tensile deformation of annealed cp-Ti.
- The orientation estimated elastic stiffness was lower in basal/near-basal grains during tensile deformation of annealed cp-Ti.
- The basal/near-basal grains/orientations had highest Taylor factor followed by off-basal & non-basal grains/orientations.
- Improved mechanical properties were observed in annealed cp-Ti where volume fraction of basal/near basal orientations/grains was higher.

SCOPE FOR FURTHER WORK

In the present study we found that texture had strong influence on mechanical properties of cp-Ti. Also texture is highly dependent on processing parameters. Hence, it may be tried to improve the texture in all angular directions of Ti sheets so that the mechanical properties will be uniform in all directions. This may be achieved by cross rolling and subsequent heat treatments..

6.0 REFERENCES

1. Askeland, D. R. "The Science and Engineering of Materials." In The Science and Engineering of Materials, by D. R. Askeland, 443. 2007.

2. ASM Metals Handbook: Fatigue and Fracture. Vol. 19. ASM Handbook, 2003.

3. Boehlert, C. J., C. J. Cowen, S. Tamirisakandala, D. J. McEldowney, and D. B. Miracle. "In situ scanning electron microscopy observations of tensile deformation in a boron-modified Ti-6Al-4V alloy." Scripta Materialia 55, no. 5 (September 2006): 465-468.

4. Eylon, D., A. Vessel, Y. Combres, R. R. Boyer, P. J. Bania, and R. W. Schutz. Journal of Metals 46 (1994): 14-16.

5. Filip, R., K. Kubiak, W. Ziala, and J. Sieniawski. "The effect of microstructure on the mechanical properties of Ti •]6Al •]4V." International Journal of fatigue 21 (1999): 679-685.

6. Froes, F. H., T. Yau, and H. G. Weidenger. "Ti, Zirconium and Hafnium." Chap. 8 in Materials Science and Technology: Structure and Properties of Nonferrous Alloys, by F. H. Froes, T. Yau and H. G. Weidenger, edited by K. H. Matucha, 401. 1996.

7. Howard, E. Boyer, ed. Hardness testing. ASM International, 1987.

8. Kuruvilla, M., and T. S. Srivatsan. Key Engineering Materials 378-379 (2008): 271-298.

9. "Processing and Fabrication of Advanced." Proceeding of Sixteenth International Symposium. Singapore, 2007. 370-388.

10. Lee, E. W., S. Lee, N. J. Kim, and J. Oh. "Correlation of fatigue properties and microstructure in investment cast Ti-6Al-4V welds." Materials Science and Engineering A 340 (2003): 232-242.

11. Li, Y. G., M. H. Loretto, D. Rugg, and W. Voice. "Acta Materialia." 49 (2001): 3011-3017.

12. M. J. Donachie, Jr. Ti- a technical guide. Second Edition. 2000.

13. Morrissey, R. J., D. L. McDowell, and T. Nicholas. "Frequency and stress ratio effects in high cycle fatigue of Ti •]6Al •]4V." International Journal of fatigue 21 (1999): 679-685.

14. Osman, E., T. Troy, L. Ying, M. Wes, and L. J. Enrique. "Enhanced tensile strength and high ductility in cryomilled commercially pure Ti." Scripta Materialia 60, no. 7 (April 2009): 586-589.

15. Paulo de campos, P., and J. C. Bressiani. Materials research 8, no. 4 (April 2005): 440-443.

16. Peter, M., A. Gysler, and G. Lutjering. Metallurgical Transactions 15A (1984): 597-605.

17. Peters, J. O., and R. O. Ritchie. "Foreign •]object damage and high cycle fatigue: role of microstructure in Ti-6Al-4V." International Journal of Fatigue 23 (2001): 413-421.

18.Schutz R. W., Thomas D. E.: Corrosion, Metals Handbook, 9th edn, Vol. 13, ASM, Metals Park, USA, (1987) p. 669

19. Sakurai K., Itabashi Y., Komatsu A.: *Ti '80, Science and Technology*, AIME, Warrendale, USA, (1980) p. 299

20.Boyer R., Welsch G., Collings E. W., eds.: *Materials Properties Handbook: Ti Alloys*, ASM, Materials Park, USA, (1994) p. 228

21.Zarkades A., Larson F. R.: The Science, Technology and Application of Ti, Pergamon Press, Oxford, UK, (1970) p. 933

22.Boyer R., Welsch G., Collings E. W., eds.: *Materials Properties Handbook: Ti Alloys*, ASM, Materials Park, USA, (1994) p. 247

23.Bunge, H.-J., *Int. Met. Rev.* 32 (1987) 265.

24.Goehner, R.P. and Michael, J.R., J., *Res. Natl. Inst. Stand. Technol.* 101 (1996) 301

25.Michael, J., in *Electron Backscatter Diffraction in Materials Science* (Eds. A.J. Schwartz, M. Kumar, and B.L. Adams), Kluwer Academic/Plenum Publishers, New York (2000) 75.

26.Small, J.A. and Michael, J.R., J. Microsc. 201 (2001) 59.

27.Wilkinson, A.J. and Hirsch, P.B., Micron 28 (1997) 279.

28.El-Dasher, B.S., Adams, B.L., and Rollett, A.D., Scr. Mater. 48 (2003) 141.

29.Introduction to texture analysis by Engler & Randle

30.Nanoindentation by Anthony C Frischer Cripps